Experimental determination of deformation potentials and band nonparabolicity parameters for PbSe

Huizhen Wu,[1] Ning Dai,[2] and Patrick J. McCann[1]*
[1]*School of Electrical and Computer Engineering, University of Oklahoma, Norman, Oklahoma 73019*
[2]*Department of Physics and Astronomy, University of Oklahoma, Norman, Oklahoma 73019*
(Received 22 January 2002; published 9 July 2002)

Parabolic IV–VI multiple-quantum well structures were grown on $BaF_2(111)$ substrates by molecular beam epitaxy and characterized by differential Fourier transform infrared transmission spectroscopy. To reduce unwanted Fabry–Perot interference fringes, the top surface of the parabolic MQW samples was coated with an antireflection film enabling unambiguous observation of subband transitions without superimposed interference fringes. Up to six principle quantized electron and hole transitions were observed. In contrast to III–V quantum well systems, the "forbidden" $\Delta n=2$ quantum transitions are not observed in the IV–VI parabolic wells. Compared with the strain effect, the quantum size effect dominates the splitting of the degeneracy of the normal and oblique valleys at the L-point in the Brillouin zone. Intervalley splitting energies and the spacings of the principle energy levels in the parabolic wells allowed determination of the deformation potential constants for PbSe, $D_d=6.1$ eV and $D_u=-1.3$ eV. From the fitting to the high-quantized energy levels observed in the differential transmission spectra, the nonparabolicity parameters for conduction and valence bands of PbSe are determined to be 1.9×10^{-15} cm^2.

DOI: 10.1103/PhysRevB.66.045303 PACS number(s): 78.66.Li

I. INTRODUCTION

Direct interband transitions in IV–VI materials occur at the four equivalent L-points in the Brillouin zone. When IV–VI multiple quantum well (MQW) structures are grown on (111)-oriented substrates one L-valley lies along the [111] growth direction, or is normal to the (111) plane in reciprocal space, and the other three are at oblique angles. Two different effective masses thus exist for potential variation along the [111] direction, one for the single normal valley $m_{111}^{\text{normal}}=m_l$, and one for the three oblique valleys $m_{111}^{\text{oblique}}=9m_lm_t(8m_l+m_t)$, where m_l and m_t are the longitudinal and transverse effective masses, respectively, associated with the prolate ellipsoids of revolution that define the constant energy surfaces for electrons and holes.[1] For IV–VI quantum wells (QWs) grown on (111)-oriented substrates the quantum size effect will thus remove L-valley degeneracy in which the N-valley [normal to the (111) plane in **k** space] is at a lower energy than the threefold degenerate O-valleys [oblique to the (111) plane in **k** space]. Unambiguous observation of subband transitions and degeneracy removal of normal and oblique L-valleys in IV–VI square QWs grown on (111)-oriented BaF_2 substrates was recently reported.[2] L-valley degeneracy removal, in which one valley is lower in energy than the other three, is a feature that is beneficial for laser applications of these IV–VI materials. The approximate fourfold reduction in the density of the lowest excited states reduces the excitation threshold for population inversion. Results from testing of recently fabricated vertical cavity surface-emitting lasers (VCSELs) made from IV–VI materials on (111) BaF_2 provide evidence for this threshold reduction. VCSELs without QWs in the active region had a minimum optical pumping threshold of 69 kW/cm^2,[3] while similarly fabricated VCSELs with QWs had thresholds as low as 10.5 kW/cm^2.[4] The more than sixfold reduction in lasing threshold is likely due in part to the fourfold reduction in the density of the lowest excited states.

Compared to more studied III–V or II–VI semiconductor QWs, however, knowledge of the physical properties of IV–VI semiconductors is still incomplete. For instance, reliable experimental data for deformation potential constants for PbSe are still not available, and thus strain effects on low dimensional structures and devices cannot be fully evaluated.[5,6] Due to the fragility of IV–VI materials, it is difficult to apply directly uniaxial stress in the crystals. Further, presence of nonparabolicity of the multiple valleys in the narrow gap IV–VI materials complicates optical investigations, particularly in the mid-infrared range. In narrow band gap semiconductors the band nonparabolicity effects on optical transitions in QW cannot be neglected, particularly for higher quantized energy levels. Krenn *et al.*[7] investigated the influence of nonparabolic-energy-band dispersion on the optical constants close to the fundamental absorption in PbSe and PbMnSe. However, up to now very little work studying the nonparabolicity effect in IV–VI QW materials has been reported, partly due to the difficulty in observing high-quantized energy level optical transitions because of Fabry–Perot interference fringes in epitaxially-grown samples. The nonparabolicity parameters for the conduction and valence bands, γ_c and γ_v, of IV–VI semiconductors have not been determined experimentally. In this work, a number of IV–VI (PbSe/PbSrSe) parabolic MQW samples have been grown as part of an effort to investigate these effects. To reduce unwanted Fabry–Perot interference fringes, the top surface of each parabolic MQW sample was coated with an antireflection film, enabling unambiguous observation of subband transitions without superimposed interference fringes. Results enable the study of quantum size, strain, and band nonparabolicity effects in the PbSe/PbSrSe parabolic QWs.

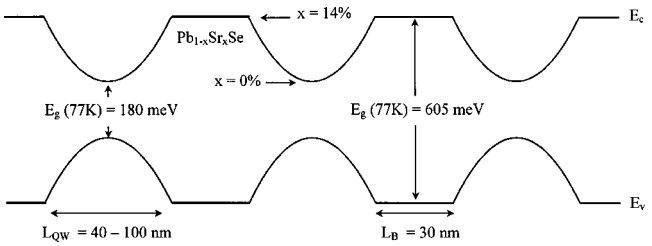

FIG. 1. Schematic band diagram for the parabolic PbSe/PbSrSe multiple quantum well structures grown by MBE. Strontium content, x, in the $Pb_{1-x}Sr_xSe$ ternary alloy varied from 0 to 14%, and each sample had between 8 and 10 quantum wells.

II. EXPERIMENT

PbSe/PbSrSe parabolic MQWs were grown on freshly cleaved $BaF_2(111)$ substrates at 400 °C in a solid source MBE system. Before the growth of the PbSe/PbSrSe MQW structures, a thin 500 Å PbSrSe buffer layer was deposited. To achieve an effective parabolic Sr compositional gradient inside each well, the wells were grown digitally using the recipe described in Ref. 8. Well widths varied from 400 Å to 1000 Å and barrier thicknesses were held constant at 300 Å. Each well contained 21 layers of PbSe and 20 layers of $Pb_{1-x}Sr_xSe$. The relative thicknesses of the $Pb_{1-x}Sr_xSe$ layers increased quadratically with distance from the well centers while that of the PbSe well layers decreased. A 5.4% Sr-to-PbSe flux ratio was used for the growth of $Pb_{1-x}Sr_xSe$ layers. Earlier work found that the alloy composition should be ~2.6 times higher (i.e., $x \sim 14\%$).[9] This produces potential barrier heights of ~200 meV at room temperature for both conduction and valence band wells assuming equal band edge discontinuities. Fourier transform infrared (FTIR) measurements showed that the absorption band gap for the $Pb_{0.86}Sr_{0.14}Se$ ternary alloy is 0.605 eV at 77 K, giving a band gap difference between $Pb_{0.86}Sr_{0.14}Se$ and PbSe of 0.425 eV. The average $Pb_{1-x}Sr_xSe$ layer thickness in the parabolically graded wells is about 10 Å, thin enough to allow electron and hole tunneling, which effectively averages the potential variation to parabolic profiles. High-resolution x-ray diffraction (HRXRD) measurements of the MBE-grown MQW structures showed numerous satellite peaks. Satellite peak spacings were used to calculate QW thicknesses, and measured values agreed with growth design values within 3%. A schematic band diagram for the parabolic PbSe/PbSrSe MQW structures is shown in Fig. 1. The number of QWs varied from 8 to 10, and typical total layer thicknesses varied from 0.8 μm to 1.0 μm.

A BioRad (FTS-60) FTIR spectrometer was used to measure transmission as a function of photon energy over a 700 cm^{-1} to 6000 cm^{-1} spectral range. Sample temperature was varied from 77 to 300 K. Unwanted Fabry–Perot interference fringes were suppressed by coating the top surface of the MQW samples with a NiCr anti-interference film.[10] Differential spectra were obtained by taking the difference between a transmission spectrum at one temperature and the spectrum at a slightly lower temperature. This takes advantage of the temperature dependence of the PbSe band gap so that step edges associated with transitions in the transmission spectra become peaks in the difference spectra. Temperature difference spectra are in essence energy derivative spectra. The temperatures of the two transmission spectra were chosen so that the shift of the PbSe band gap was 1 meV. (Thus an energy resolution of 1 meV is maintained in this process.) An advantage of the differential spectrum is that it greatly reduces the residual Fabry–Pérot fringe interference since the dielectric constants of the materials are very weakly dependent on temperature. The direct gap in the $Pb_{0.86}Sr_{0.14}Se$ barrier alloy observed in the transmission spectra is used as a parameter for calculations of quantized electronic transitions. More details of the differential FTIR transmission measurements are described in Ref. 2.

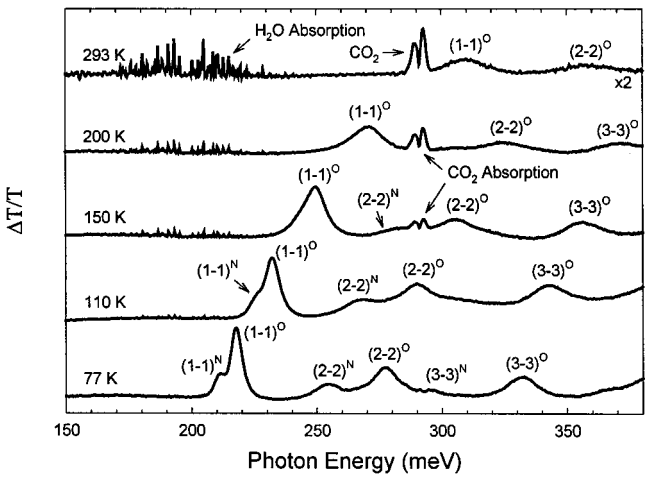

FIG. 2. FTIR differential transmission spectra for a parabolically graded PbSe/PbSrSe MQW sample with well widths of 600 Å and PbSrSe barrier widths of 300 Å measured at different temperatures. Two longitudinal valley subband transitions, $(1-1)^N$, $(2-2)^N$, and three oblique valley subband transitions, $(1-1)^O$, $(2-2)^O$, and $(3-3)^O$ are unambiguously revealed.

III. RESULTS AND DISCUSSION

A. Quantum size effect

Figure 2 shows temperature dependent differential transmission spectra for a ten-period MQW sample with parabolic well widths of 600 Å and PbSrSe barrier widths of 300 Å. These differential spectra exhibit peaks associated with transitions from different conduction and valence band valleys. These peaks are purely excitonic at low temperatures and band-to-band at higher temperatures.[11] The difference between the excitonic and band gap energies can be neglected because of the very small exciton binding energies (a hydrogenic model gives a value of about 0.007 meV) in these high dielectric constant IV–VI materials. As electrons (and holes) in the N-valley of PbSe have a larger effective mass than electrons (and holes) in the O-valleys, see Table I, the lowest energy peak at 211 meV shown in the 77 K spectrum is due to the first N-valley subband transition, $(1-1)^N$, while the next peak at 217 meV is due to the threefold degenerate O-valley subband transitions, $(1-1)^O$. In the case of square quantum wells similar transitions were also observed.[2] The energy spacing between sequential N-valley transitions is

TABLE I. PbSe band structure parameters used in the calculations of quantized states of electrons and holes in parabolic PbSe/PbSrSe MQW structures. All values are for PbSe at 77 K and m_0 is the mass of a free electron.

Band structure parameters for PbSe at 77 K								
E_g	$m_{l,e}$	$m_{t,e}$	$m_{l,h}$	$m_{t,h}$	m_e^{N}	m_e^{O}	m_h^{N}	m_h^{O}
meV	m_0	m_0	m_0	m_0	m_0	m_0	m_0	m_0
180	0.0788	0.0475	0.0764	0.0386	0.0788	0.0475	0.0764	0.0408

smaller than that between sequential O-valley ones. Assignments of the various subband transitions are indicated in Fig. 2, and the superscripts indicate whether the electron and hole states involved are derived from N- or O-valleys. As seen in Fig. 2 the differential spectra are dominated by oblique valley transitions because oblique valleys are threefold degenerate and have larger transition matrix elements. A comparison of the integrated intensities for the $(1-1)^{\mathrm{N}}$ and $(1-1)^{\mathrm{O}}$ peaks reflects the difference in the joint density of states between these two transitions.

Identification of the other allowed $(2-2)^{\mathrm{N}}$, $(2-2)^{\mathrm{O}}$, and $(3-3)^{\mathrm{O}}$ transitions marked in Fig. 2 is assisted by considering fact that for an ideal parabolic well the quantum state levels should have equal spacings. These attributions are also consistent with the integrated intensities of the differential peaks; peak areas for O-valley transitions are about three times those for N-valley transitions. The spacings between $(2-2)^i$ and $(1-1)^i$ transitions are 42 meV for the N-valley and 60 meV for the O-valley. However, as seen from Fig. 2 these spacings decrease when the quantized energy levels increase. In contrast to III–V semiconductors, all subband transitions shift to higher energies as temperature increases due to the fact that PbSe has a positive temperature coefficient ($dE_g/dT>0$). Peak broadening at elevated temperatures is due to increasing electron–phonon scattering.

For parabolic potential functions the energy levels for allowed electron (or hole) states depend on well width, L_{QW},

$$E_{nj}^{i}=2\left(n-\frac{1}{2}\right)\frac{\hbar}{L_{\mathrm{QW}}}\sqrt{\frac{2Q_c\Delta E_g}{m_e^*}}, \tag{1}$$

where $n=1,2,3,...,m_e^*$ is the electron (or hole) effective mass, and ΔE_g is the total energy gap difference from the bottom of the wells to the top of the wells, 425 meV at 77 K as measured by FTIR transmission. Q_c is the fraction of ΔE_g for the conduction band well. Prior work has shown that conduction and valence band edge discontinuities in IV–VI QWs are approximately equal,[12,13] so a value of Q_c of 0.5 is used here. At 77 K, the effective masses for electrons and holes in the N- and O-valleys are obtained from Ref. 14, see Table I. Subband transition energies in the parabolic MQWs can be calculated using Eq. (1). If the nonparabolicity of PbSe is not considered, calculation from Eq. (1) showed the energy spacings between sequential N- and O-valley quantum transitions for the 600 Å parabolic wells to be 43 and 58 meV, respectively. These values are in good agreement with the observed data from Fig. 2, 42 meV for the N-valley and 60 meV for the O-valleys. However, comparison of calculated ground state transition energies, $(1-1)^i$ ($i=\mathrm{N,O}$), with the observed transition energies shown in Fig. 2 gives discrepancies for both N- and O-valleys as large as 10 meV. The calculated N-valley transition energy $(1-1)^{\mathrm{N}}$ is at 201.5 meV, while the observed one is at 210.7 meV, i.e., the measured transition energy is 9.2 meV higher than the calculated one. For O-valley $(1-1)^{\mathrm{O}}$ transitions, the calculated value is 209.0 meV, while the observed result is 217.6 meV, 8.6 meV higher than theory predicts. The comparison of other samples considered here showed similar discrepancies. A reason for the disagreements includes band gap enlargement due to the strain effect involved in the well layers. This issue will be discussed in the next section.

Figure 3 shows differential transmission spectra at 77 K for four parabolic MQW samples with well widths of 400 Å, 600 Å, 800 Å, and 1000 Å. The optical transitions related to many high-quantized energy levels are observed in the wide-well samples. In the sample with parabolic well widths of 1000 Å up to six, $(6-6)^{\mathrm{O}}$, transitions are observed. As the well width decreases, both the splitting between the $(i-i)^{\mathrm{N}}$ and the $(i-i)^{\mathrm{O}}$ transitions and the energy spacings of sequential quantum transitions increase. Again, in all three samples the O-valley transitions $(i-i)^{\mathrm{O}}$ dominate the spectra because of the three fold degeneracy of the oblique valleys. In III–V parabolic wells both ''allowed'' $\Delta n=0$ (where n is the subband index) and ''forbidden'' $\Delta n=2$ absorptions transitions are observed.[8,15] However, in the case of IV–VI quantum

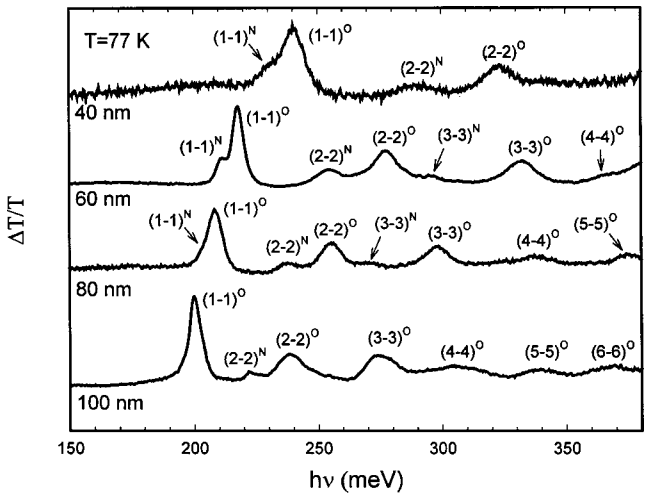

FIG. 3. FTIR differential transmission spectra for four parabolically graded MQW samples with well widths of 400 Å, 600 Å, 800 Å, and 1000 Å at 77 K. As the well width decreases the splitting between $(i-i)^{\mathrm{N}}$ and $(i-i)^{\mathrm{O}}$ increases.

wells, the ''forbidden'' transitions have not been observed in either parabolic MQWs or square MQWs.[2,5]

B. Strain effect

From the above discussion, it is seen that the discrepancy between the calculated and measured peak positions for $(1-1)^i$ is as large as 10 meV, though the energy spacings between sequential N- and O-valley quantum transitions are in reasonable agreement. The reason of the absolute energy level discrepancies is due to the following factors. First, strain effects due to lattice and thermal expansion mismatches between different materials in the PbSe/PbSrSe system can enlarge the band gap of the PbSe well layer and shift the ground states of both the normal and oblique valleys to higher energies. However, the band gap enlargement due to strain in the stressed parabolic well layers has a small effect, <1 meV, on the energy difference between sequential quantized energy levels. Band nonparabolicity of PbSe will also contribute to change in quantized energy levels, particularly on higher quantum numbers, but not on ground state transitions, $(1-1)^i$ $(i=\mathrm{N,O})$. The following discussion will focus on how strain can affect observed transitions.

Strain effects on the optical transitions in the parabolic MQWs can be understood by calculating the strain induced by the lattice mismatch as well as the thermally induced strain due to the differences between the thermal expansion coefficients of the substrate and the epilayers. The lattice mismatch between PbSe and the BaF_2 substrate is 1.2% at room temperature. Since the epilayers are ~ 1 μm thick and the critical layer thickness is <100 Å, it can be expected that PbSe/PbSrSe epilayers are fully relaxed and they stand freely on the BaF_2 substrate.[5] A linear interpolation between PbSe and SrSe lattice parameters (6.126 Å and 6.243 Å, respectively) gives a lattice constant of 6.144 Å for the $Pb_{0.86}Sr_{0.14}Se$ barrier layers, which has a 0.29% lattice mismatch with the PbSe wells. This produces tensile strain in PbSe and compressive strain in PbSrSe. Such tensile strain is expected to increase the band gap and possibly induce additional splitting of the degeneracy of the normal and oblique valleys.[5] The difference of thermal expansion coefficients between PbSe and BaF_2 is small, therefore, the strain due to thermal expansion mismatch between the substrate and epilayers can be neglected. Thermal expansion data for PbSrSe are not available, but the concentration of Sr in the PbSrSe layers is low, so it is reasonable to neglect the difference of thermal expansion coefficients between the PbSe and PbSrSe materials used in the structures.

Strain in the parabolically graded quantum wells will vary with Sr content. Because the maximum lattice mismatch between PbSe and PbSrSe is small, $<0.3\%$, the full tensile strain throughout the well layers is assumed. In the case of epilayers freely standing on a substrate, the in-plane strain has the form,

$$\varepsilon_{\parallel}=\frac{(a_2-a_1)d_2}{a_1(d_1+d_2)}. \tag{2}$$

Here a_1, a_2 and d_1, d_2 are the lattice constants and layer thicknesses for the two component materials, respectively. The thicknesses of the PbSe and PbSrSe layers are obtained from the digital growth data. In PbSe, which has an fcc crystal structure, $\varepsilon_{\parallel}$ and $\varepsilon_{\perp}$ in the (111) orientation have the relation,

$$\varepsilon_{\perp}=-2\frac{C_{11}+2C_{12}-2C_{44}}{C_{11}+2C_{12}+4C_{44}}\varepsilon_{\parallel}. \tag{3}$$

The change of the band gap due to tensile strain[16] for the N-valley of PbSe is

$$\delta E_g^{\mathrm{N}}=2\left(\frac{6C_{44}}{C_{11}+2C_{12}+4C_{44}}D_d - \frac{C_{11}+2C_{12}-2C_{44}}{C_{11}+2C_{12}+4C_{44}}D_u\right)\varepsilon_{\parallel}, \tag{4}$$

and for the O-valleys is

$$\delta E_g^{\mathrm{O}}=2\left(\frac{6C_{44}}{C_{11}+2C_{12}+4C_{44}}D_d + \frac{1}{3}\frac{C_{11}+2C_{12}+6C_{44}}{C_{11}+2C_{12}+4C_{44}}D_u\right)\varepsilon_{\parallel}, \tag{5}$$

where $D_d=D_d^c-D_d^v$ and $D_u=D_u^c-D_u^v$ are the differences between conduction and valence band deformation potentials; $\varepsilon_{\parallel}$ is the in-plane strain; C_{11}, C_{12}, and C_{44} are elastic constants that are quoted from Ref. 17. Equations (4) and (5) show that the first term contributes to elevation of both of the N- and O-valleys by the same amount, while the second term contributes to the splitting of the two different valleys.

The observed differential spectra, Figs. 2 and 3, can yield values for δE_g^{N} and δE_g^{O}. The energy levels of electrons in a parabolic potential well are equally spaced according to Eq. (1). This spacing, ΔE_{HO}, which is denoted with the subscript ''HO'' since it corresponds to the same energy spacing between eigenvalues for a harmonic oscillator, is expressed by the following equation:

$$\Delta E_{\mathrm{HO}}=\frac{1}{2}[E_{(2-2)}-E_{(1-1)}]=\frac{\hbar}{L_{\mathrm{QW}}}\sqrt{\frac{2Q_c\Delta E_g}{m_e^*}}. \tag{6}$$

The energy level spacing can be experimentally determined by taking one-half of the difference between the first and second transition energies. This implies symmetric conduction and valence band curvatures, which is a reasonable assumption based upon similar electron and hole effective masses, see Table I. Figure 4 shows the energies involved in this analysis. Since the first bound states are above the bottom of the conduction band and below the top of the valence band by $\frac{1}{2}\Delta E_{\mathrm{HO}}$, the band gap energy of PbSe in the MQW structure can be measured by taking the energy level of the ground state transition and subtracting the energy level spacing, ΔE_{HO}, as determined from the differential transmission spectra. Further subtraction of the bulk band gap energy will yield the change in band gap, δE_g^{N} or δE_g^{O}, due to tensile strain in the PbSe layer caused by the larger lattice parameter $Pb_{0.86}Sr_{0.14}Se$ barrier alloy in the MQW structure,

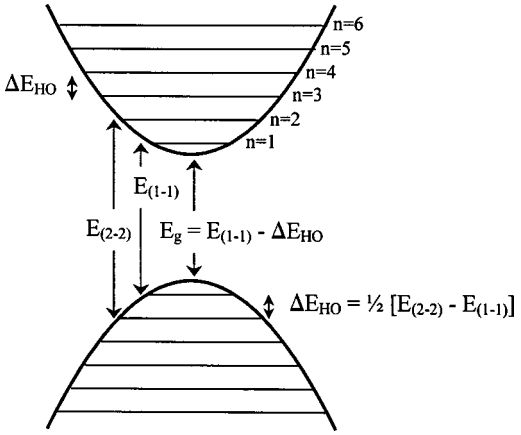

FIG. 4. Depiction of uniform energy level spacing for electrons and holes in the parabolic potential wells of a compositionally-graded $Pb_{1-x}Sr_xSe$ quantum well. Peaks in the measured differential absorption spectra correspond to interband transitions as indicated by the $E_{(1-1)}$ and $E_{(2-2)}$ energies.

$$\delta E_g^{\mathrm{N}} = E_{(1-1)^{\mathrm{N}}} - \Delta E_{\mathrm{HO}^{\mathrm{N}}} - E_g(\mathrm{bulk}), \tag{7}$$

$$\delta E_g^{\mathrm{O}} = E_{(1-1)^{\mathrm{O}}} - \Delta E_{\mathrm{HO}^{\mathrm{O}}} - E_g(\mathrm{bulk}). \tag{8}$$

Up to now reliable deformation potential values for PbSe have not been available. Using the elastic constants at 77 K quoted in Ref. [15], measured δE_g^N and δE_g^{O} values from the spectra for the four different samples shown in Fig. 3, and the strain obtained from Eq. (2), it is possible to calculate the deformation potentials of PbSe. From Eq. (2) and the thicknesses of PbSe and $Pb_{0.86}Sr_{0.14}Se$, the strain for the sample with well width of 400 Å is 0.19%, and for the sample with well width 1000 Å is 0.14%. Only the differences between the two peak position pairs, $(2-2)^{\mathrm{N}}$ and $(1-1)^{\mathrm{N}}$ or $(2-2)^{\mathrm{O}}$ and $(1-1)^{\mathrm{O}}$ in each spectrum were used in this determination of the deformation potential constants. These transition energies were used because the ground state and first excited state energies are the least affected by band nonparabolicity effects. The following deformation potential constants are thus obtained: $D_d = 6.1$ eV and $D_u = -1.3$ eV, see Table II. These two constants are in reasonable agreement with values obtained from augmented plane wave (APW) calculations,[18] $D_d = 6.48$ eV and $D_u = -2.11$ eV.

The differential spectra of the parabolic quantum well structures also provide a valuable way to distinguish the subband transition changes due to the quantum size effect from changes due to lattice deformation. Another interesting result observed in Fig. 3 is that the splitting of the degeneracy of the two valleys, $(1-1)^{\mathrm{N}}$ and $(1-1)^{\mathrm{O}}$ is mainly due to the quantum size effect rather than the strain effect. This is because the contribution from the second terms in Eqs. (4) and (5) is small. For the sample with parabolic well widths larger than 1000 Å almost no splitting between $(1-1)^{\mathrm{N}}$ and $(1-1)^{\mathrm{O}}$ is observed, though the strain in the wells is not significantly different from thinner well samples.

TABLE II. Experimentally derived deformation potentials and nonparabolicity coefficients for PbSe at 77 K.

Experimentally derived parameters for PbSe			
D_d	D_u	γ_c	γ_v
eV	eV	cm^2	cm^2
6.1	−1.3	1.9×10^{-15}	1.9×10^{-15}

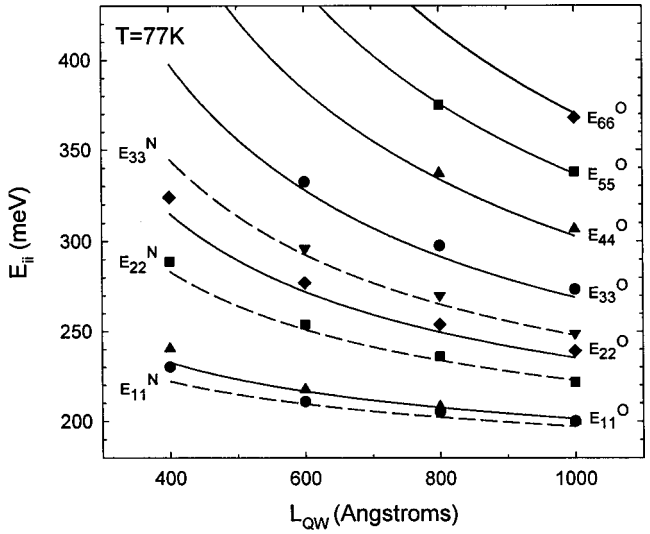

FIG. 5. The observed subband transition energies versus well width of parabolic PbSe/PbSrSe MQWs at 77 K. The dashed lines are the calculated energies for N-valley transitions, $(i-i)^{\mathrm{N}}$, and the solid lines are for O-valley transitions, $(i-i)^{\mathrm{O}}$, obtained with the deformation potential constants $D_d = 6.1$ eV, $D_u = -1.3$ eV and nonparabolicity parameters $\gamma_{c,v} = 1.9\times10^{-15}$ cm^2.

C. Band nonparabolicity effect

The measured energies for different quantized state transitions are plotted in Fig. 5. It is seen that for all quantum well thicknesses as optical transition energies increase the energy spacing between the higher quantized states becomes smaller. The reduced energy spacing between the more excited states is proportional to quantum state number. The observed diminishing of the energy spacing for the more excited electron and hole states is due to band nonparabolicity effects in the quantum well. For narrow gap semiconductors, such as IV–VI materials, band nonparabolicity effects cannot be neglected, particularly for higher quantized levels. In III–V materials, band nonparabolicity effects have been considered by introducing an energy-dependent effective mass $m_w^*(E_z) = m_w^*(1 + 2E_z/E_g)$, where m_w^* is the effective mass at the bottom of the conduction band and E_g is the band gap of the well layers. However, in IV–VI materials, this approach is not viable due to the small E_g.

According to Kane's model, the conduction and valence band energies can be expressed up to k^4 in terms of nonparabolicity parameters γ_c and γ_v, respectively, as

$$E_c = \frac{\hbar^2 k^2}{2m_c}(1 - \gamma_c k^2), \tag{9}$$

$$E_v = \frac{\hbar^2 k^2}{2m_v}(1-\gamma_v k^2). \tag{10}$$

According to the definition of energy-dependent effective mass, $m_w^*(E_z)=\hbar^2 k\partial k/\partial E_z(k)$, and using (9) and (10) we obtain the energy dependent effective masses of the well layers,

$$m_w^*(E_z) = m_w^* \frac{1}{\sqrt{1-\dfrac{8m_w^*\gamma_c E_z}{\hbar^2}}}, \tag{11}$$

$$m_w^*(E_z) = m_w^* \frac{1}{\sqrt{1-\dfrac{8m_w^*\gamma_v E_z}{\hbar^2}}}. \tag{12}$$

To the authors' knowledge, the nonparabolicity constants γ_c and γ_v for PbSe have not been experimentally determined. It is known that the band structure for PbSe at the L-point is symmetric for both conduction and valence bands, so $\gamma_c = \gamma_v$, which allows us to use the interband transition energies to determine the nonparabolicity parameters. Substituting the energy dependent mass into (1) and using γ_c and γ_v, as parameters to fit the experimental data (shown in Fig. 5), the subband transitions for both normal and oblique valleys were obtained. The results are plotted as lines in Fig. 5. It is seen that the calculated values are in reasonably good agreement with the optical transition energies measured by differential FTIR. The nonparabolicity constants for both the conduction and valence bands of PbSe, $\gamma_c=\gamma_v=1.9\times10^{-15}$ cm^2, are thus obtained, see Table II. Figure 6 shows the comparison of the conduction and valence band energy dispersions, $E_c(k)$ and $E_v(k)$ with the experimentally determined γ_c and γ_v values to those of parabolic bands. It is seen that the nonparabolicity effect is significant for electrons or holes excited by more than ~250 meV with respect to the conduction or valence band edges, respectively.

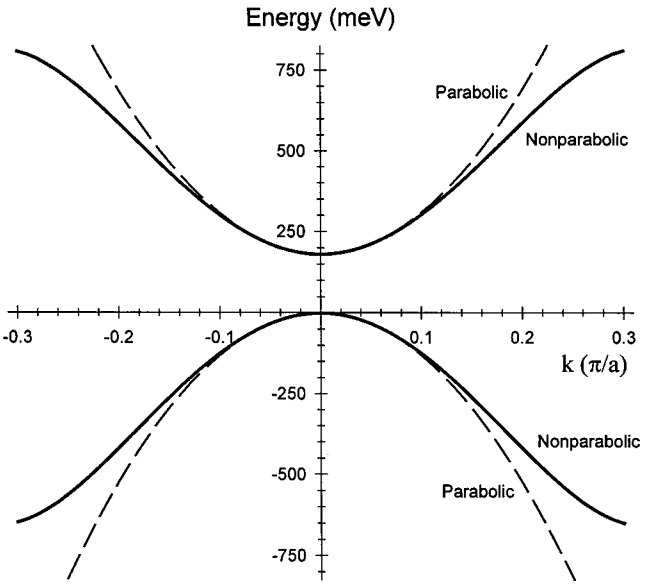

FIG. 6. Energy vs momentum ($E_{c,v}$ vs k) relationship for electrons and holes in PbSe. The nonparabolic relationship (solid line) was obtained using Eq. (5) and the experimentally determined γ_c and γ_c values. A parabolic E vs k relationship (dashed line) is shown for reference.

IV. CONCLUSIONS

Parabolic PbSe/PbSrSe multiple-quantum well structures were grown on $BaF_2(111)$ substrates by molecular beam epitaxy. Unambiguous observation of subband transitions by differential FTIR spectra without superimposed interference fringes revealed the expected harmonic oscillator energy levels. High-order quantized electron and hole transitions up to $(6-6)^O$ were observed. In contrast with III–V quantum well systems, the ''forbidden'' $\Delta n=2$ quantum transitions were not observed in the IV–VI parabolic wells. The quantum size effect dominates the splitting of the degeneracy of the longitudinal and oblique valleys at the L-point in the Brillouin zone. The observation of intervalley splittings and the spacings of the energy levels in the parabolic wells allowed determination of the deformation potential constants for PbSe, $D_d=6.1$ eV and $D_u=-1.3$ eV, which are in reasonable agreement with values obtained from APW calculations. From the fitting to the highly excited state transitions observed in the differential transmissions the nonparabolicity parameters for conduction and valence band of PbSe are determined to be 1.9×10^{-15} cm^2 for each band.

ACKNOWLEDGMENTS

Funding for this work was provided by the National Science Foundation, Grant Nos. DMR-9802396 and DMR-0080054.

*Author to whom correspondence should be addressed. Electronic address: pmccann@ou.edu

[1] M. F. Khodr, P. J. McCann, and B. A. Mason, IEEE J. Quantum Electron. **32**, 236 (1996).
[2] H. Z. Wu, N. Dai, M. B. Johnson, P. J. McCann, and Z. S. Shi, Appl. Phys. Lett. **78**, 2199 (2001).
[3] Z. Shi, G. Xu, P. J. McCann, X. M. Fang, N. Dai, C. L. Felix, W. W. Bewley, I. Vurgaftman, and J. R. Meyer, Appl. Phys. Lett. **76**, 3688 (2000).
[4] C. L. Felix, W. W. Bewley, I. Vurgaftman, J. R. Lindle, J. R. Meyer, H. Z. Wu, G. Xu, S. Khosravani, and Z. Shi, Appl. Phys. Lett. **78**, 3770 (2001).
[5] E. Abramof, E. A. de Andrada e Silva, S. O. Ferreira, P. Motisuke, P. H. O. Rappl, and A. Y. Ueta, Phys. Rev. B **63**, 085304 (2001).
[6] V. Valeiko, I. I. Zasavitskii, A. V. Matveenko, and B. N. Matsonashvili, Z. A. Rukhadze, Superlattices Microstruct. **9**, 195 (1991).
[7] H. Krenn, S. Yuan, N. Rank, and G. Bauer, Phys. Rev. B **57**, 2393 (1998).

[8] R. C. Miller, A. C. Gossard, D. A. Kleinman, and O. Munteanu, Phys. Rev. B **29**, 3740 (1984).
[9] A. Lambrecht, N. Herres, B. Soanger, S. Kuhn, H. Böttner, M. Tacke, and J. Evers, J. Cryst. Growth **108**, 301 (1991).
[10] S. W. McKnight, K. P. Stewart, H. D. Drew, and K. Moorjani, Infrared Phys. **27**, 327 (1987).
[11] W. Z. Shen, H. Z. Wu, and P. J. McCann, J. Appl. Phys. **91**, 3621 (2002).
[12] Erasmo A. de Andrada e Silva, Phys. Rev. B **60**, 8859 (1999).
[13] S. Yuan, G. Springholz, G. Bauer, and M. Kriechbaum, Phys. Rev. B **49**, 5476 (1994).
[14] Landolt-Börnstein, in *Numerical Data and Functional Relationships in Science and Technology*, edited by O. Madelung (Springer, Berlin, 1987), Vol. 17.
[15] N. Dai, G. A. Khodaparast, F. Brown, R. E. Doezema, S. J. Chung, and M. B. Santos, Appl. Phys. Lett. **76**, 3905 (2000).
[16] J. Singleton, E. Kress-Rogers, A. V. Lewis, R. J. Nicholas, E. J. Fantner, G. Bauer, and A. Otero, J. Phys. C **19**, 77 (1986).
[17] H. Zogg, S. Blunier, A. Fach, C. Maissen, P. Muller, S. Teodoropl, V. Meyer, G. Kostorz, A. Dommann, and T. Richmond, Phys. Rev. B **50**, 10 801 (1994).
[18] Sohrab Rabii, Phys. Rev. **167**, 801 (1968).